atmosphere

MDPI

Article

Investigating the Large-Scale Transport of a Volcanic Plume and the Impact on a Secondary Site

David Jean Du Preez [1,2,*], Hassan Bencherif [2,3], Nelson Bègue [2], Lieven Clarisse [4], Rebecca F. Hoffman [5] and Caradee Yael Wright [1,6]

1 Department of Geography, Geoinformatics and Meteorology, University of Pretoria, Pretoria 0002, South Africa; caradee.wright@mrc.ac.za
2 Laboratoire de l'Atmosphère et des Cyclones (UMR 8105 CNRS, Université de La Réunion, MétéoFrance), 97744 Saint-Denis de La Réunion, France; hassan.bencherif@univ-reunion.fr (H.B.); nelson.begue@univ-reunion.fr (N.B.)
3 School of Chemistry and Physics, University of KwaZulu-Natal, Durban 4041, South Africa
4 Spectroscopy, Quantum Chemistry and Atmospheric Remote Sensing (SQUARES), Université libre de Bruxelles (ULB), 1050 Bruxelles, Belgium; lclariss@ulb.ac.be
5 South African Weather Service, Private Bag X097, Pretoria 0001, South Africa; rebecca.hoffman@weathersa.co.za
6 Environmental and Health Research Unit, South African Medical Research Council, University of Pretoria, Pretoria 0001, South Africa
* Correspondence: dupreez.dj@tuks.co.za

Received: 21 April 2020; Accepted: 22 May 2020; Published: 25 May 2020

Abstract: Volcanic plumes can be transported across vast distances and can have an impact on solar ultraviolet radiation (UVR) reaching the surface due to the scattering and absorption caused by aerosols. The dispersion of the volcanic plume from the Puyehue-Cordón Caulle volcanic complex (PCCVC) eruption was investigated to determine the effect on aerosol loading at Cape Point, South Africa. The eruption occurred on 4 June 2011 and resulted in a plume reaching a height of between 9 and 12 km and was dispersed across the Southern Hemisphere. Satellite sulphur dioxide (SO_2) observations and a dispersion model showed low concentrations of SO_2 at the secondary site. However, satellite observations of volcanic ash and ground-based aerosol measurements did show increases between 10 and 20 June 2011 at the secondary site. Furthermore, there was good agreement with the dispersion model results and observations from satellites with most of the plume located between latitudes 40°–60° South.

Keywords: aerosols; sulphur dioxide; FLEXPART; plume transport; volcanic eruption

1. Introduction

Volcanic eruptions can eject a highly reactive mix of aerosols and gases into the atmosphere [1]. Some of the main gases associated with volcanic activity are water vapour (H_2O), carbon dioxide (CO_2), sulphur dioxide (SO_2), hydrogen sulphide (H_2S) and hydrochloric acid (HCl) [2]. Volcanic emissions are the largest natural sources of SO_2 in the atmosphere. Volcanic eruptions occur with various levels of intensity. Larger eruptions can inject volcanic aerosols into the stratosphere, while smaller, less intense eruptions only inject aerosols into the troposphere. SO_2 is suspended in the troposphere for only a short period of time, but SO_2 injected into the stratosphere through volcanic eruptions can remain there for up to three years as sulphuric acid aerosols [3,4]. The injection of ash and SO_2 from volcanic eruptions affects the climate, aviation and human health due to the deposition of ejected matter [5].

SO_2 injected into the stratosphere can be dispersed around the globe and can have an important climatic effect. Sulphur species react with hydroxide (OH) and water vapour (H_2O) to form sulfuric

acid (H_2SO_4). These H_2SO_4 aerosols have a radiative effect during eruptions [6]. Furthermore, solar ultraviolet radiation (UVR) passing through the atmosphere is affected by the aerosol loading. During volcanic eruptions the aerosol loading and size distribution are modified by injected ash particles [7]. UV-absorbing aerosols such as volcanic ash affect surface UVR flux which impact public health and some photochemical reactions. The effect of UV-absorbing aerosols on UVR is dependent on the altitude, particle size distribution and single scattering albedo of the ash particles [8].

The Puyehue-Cordón Caulle volcanic complex (PCCVC) is located in the Andes Mountains in southern Chile (40.58° S, 72.13° W) at 2 240 m above sea level [9]. After 41 years of inactivity, an eruption started on 4 June 2011 at approximately 18:30 UTC. The resulting plume reached the stratosphere with maximum heights between ~9–12 km [4,7] with a peak mean flow rate (MFR) in the order of 10^7 kg·s^{-1}. On 13 June 2011, the plume reached a height of ~7–9 km [10]. Due to the westerly winds in the mid-latitudes, widespread dispersion of aerosols and fine particles occurred across the Southern Hemisphere [11].

By 14 June 2011, the plume had circumnavigated the Southern Hemisphere and reached the original eruption site [4]. The plume was subjected to cross-wind and down-wind spreading, with most of the velocity as a result of the wind. The umbrella cloud and the rising plume were both affected by the prevailing westerly winds, showing the significant effect that the wind had on the dispersion of the aerosols and ash, although some of the spreading was due to physical processes in the plume such as density-driven mechanisms [10]. Following the initial eruption, the volcano continued to produce low-intensity plumes for several months [10].

In this study, SO_2 anomalies were identified at the eruption site as well as at a secondary site, Cape Point, South Africa was selected as the secondary site because air traffic was reportedly restricted on 18–19 June 2011 due to 'ash' from the eruption being visible at Cape Town International Airport. The secondary site was included to consider the extent of the impact of PCCVC 2011 eruption over a distance. Furthermore, the trajectory and dispersion of the plume was investigated using satellite observations and model output to determine whether the plume did reach the secondary site and whether or not SO_2 anomalies at the secondary site could be attributed to the volcanic eruption.

2. Data and Methods

2.1. Data

The eruption site, PCCVC (40.58° S; 72.11° W), and the secondary site, Cape Point (34.35° S; 18.50° E) (Figure 1) were selected to investigate the dispersion of the plume and the effect on a secondary site.

The Cape Point station is part of the Global Atmosphere Watch (GAW) network and equipment at the station is used to monitor trace gases. The station is situated 230 m above sea level and is mainly influenced by air masses from the South Atlantic Ocean due to the prevailing southeasterly winds throughout the year. During the austral winter the station may be influenced by anthropogenic emissions from local and regional biomass burning, transported by northerly winds as a result of changes in circulation patterns caused by frontal systems [12].

Daily noon ultraviolet index (UVI) data (2007–2016, inclusive) from the Ozone Monitoring Instrument (OMI) were used to determine if the volcanic plume had any impact on surface solar UVR. The OMI data has a 1° × 1° spatial resolution [13] and OMI has a spectral resolution of 0.45 nm [14]. The UVI is a scale used to represent erythemal radiation levels [15]. During the time that the plume was likely to impact surface solar UVR levels, ground-based observations of solar UVR levels at Cape Point were not available but there is known to be good agreement between the Cape Point ground-based observations and OMI data [16]. Previous studies have shown that OMI estimations of surface UVR are above the ground-based observations indicating a positive bias which is decreased under clear-sky conditions [14].

Aerosol optical depth (AOD) data (2011 to 2018, inclusive) from a precision filter radiometer (PFR) located at Cape Point were used to identify any anomalies in AOD as a result of the volcanic plume. The data for the PFR were obtained from the World Data Centre for Aerosols (WDCA) website (http://ebas.nilu.no/). The PFR sun photometer measures AOD at four wavelengths (λ = 368, 412, 500, 862 nm) and started operation in February 2008 but only data from 2011 were available. From calibration tests, the PFR located at Cape Point had an uncertainty of less than ± 1%. Hourly average AOD values were determined from 1-minute data using GAW-PFR algorithms [17,18] and cloud screening routines [19].

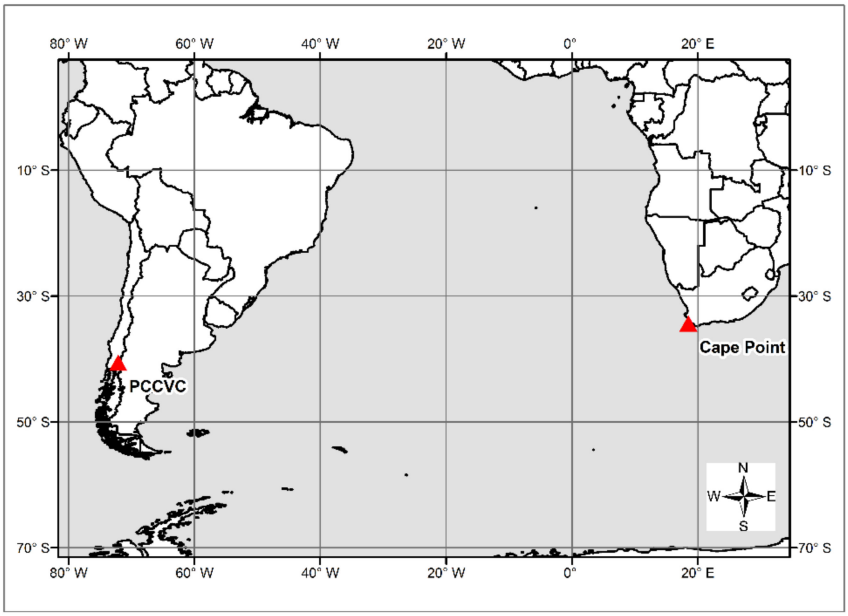

Figure 1. Map showing the location of the eruption site, Puyehue-Cordón Caulle volcanic complex in South America and the secondary site, Cape Point in South Africa [20].

Hourly reanalysis data from Modern-Era Retrospective Analysis for Research and Applications version 2 (MERRA-2) spatial resolution of 0.5° × 0.65° [21] was used to identify anomalies in SO_2 column mass density (kg·m^{-2}) (2007–2016). MERRA-2 uses observations from the Earth Observing System (EOS). The Goddard Global Ozone Chemistry Aerosol Radiation and Transport (GOCART) and Goddard Earth Observing System 5 (GEOS-5) models simulate atmospheric processes [22].

SO_2 vertical column density and volcanic ash observations were obtained from the Infrared Atmospheric Sounding Interferometer (IASI) instrument on board the MetOp-A satellite. The SO_2 is given in Dobson Units (DU) and computed using the algorithm outlined which calculates the total column SO_2 using the assumed height of the SO_2 layer and is dependent on factors from data retrieved from the instrument [23]. Volcanic ash absorbs and scatters radiation with wavelengths between 7 μm and 15 μm [24–26]. In [27] a volcanic ash identification algorithm was presented, that determines for each IASI spectral band whether a spectral signature is present that is compatible with the presence of ash. In the same study, the algorithm was illustrated on the observations of Puyehue to estimate the fraction of spectra with detectable quantities of ash. It is this dataset that is also used here.

2.2. Methods

The monthly mean UVI for June was calculated using nine-years (2007–2010, inclusive and 2012–2016, inclusive) and 2011 data were excluded to remove the possible influence of the volcanic eruption. To identify UVI anomalies during June 2011, the calculated mean UVI for June was subtracted from the mean UVI for June 2011.

Similarly, daily mean and standard deviation (SD) values were calculated for the MERRA-2 SO_2 column data at both sites. Using the PFR AOD data for 2011, the daily mean was calculated. The remaining seven years of data (2012–2018, inclusive) were used to calculate the monthly mean and SD values of the PFR AOD data at Cape Point. The mean and SD values of UVI, MERRA-2 and PFR data were compared to the 2011 observations to identify any outliers.

The flexible particle (FLEXPART) model is a Lagrangian particle dispersion model which was used to model the dispersion of the volcanic plume. The model simulates the transport, diffusion, wet and dry deposition and first order chemical reactions of tracer particles released from a point source or area source [28]. In this study, forecast meteorological data from the European Centre for Medium Range Forecasts (ECMWF) was used as input for the model. The meteorological data has a 3-hour temporal resolution, 1° × 1° spatial resolution and 138 vertical levels. In this study, no a priori information was used in the FLEXPART model simulation. Using SO_2 as a proxy for volcanic ash [29] has been done in several previous studies [4,30] and is dependent on environmental conditions [27]. A similar model setup was used as described by Klüser et al. (2013) [4], where a large number of particles of unit mass were released from 4–13 June 2011, between 2–14 km above the eruption site at 6-hour intervals [4]. The simulation was run from 1–30 June 2011 to observe the dispersion of the plume across the Southern Hemisphere. An output grid of 1° × 1° was produced every 12 h at 1 km intervals from 4–14 km and the SO_2 column given in ng·m^{-3} was converted to Dobson units.

3. Results and Discussion

3.1. Surface Ultraviolet Radiation (UVR)

The UVI anomalies for June 2011 (Figure 2) indicated changes of ± 0.5 UVI. The region between 20° S and 35° S was dominated by decreases in UVR. In the region between 40° S and 60° S, small increases and decreases in UVI were observed.

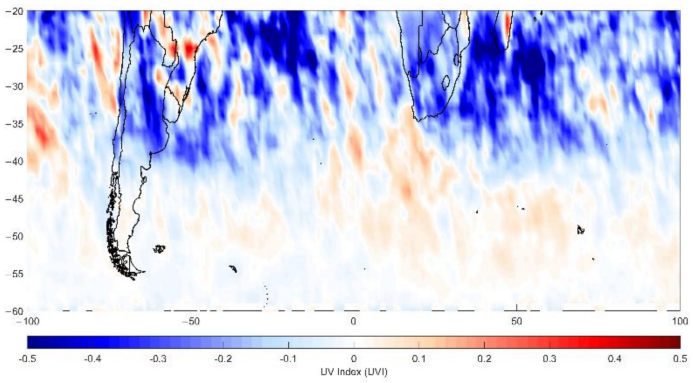

Figure 2. Ultraviolet index (UVI) anomalies for June 2011 where positive values indicate an increase in UVI and vice versa.

3.2. Aerosol Optical Depth (AOD) and SO_2 Anomalies

The monthly mean and ± 1 standard deviation (SD) of PFR AOD at 368 and 412 nm (Figure 3) showed that there was no clear seasonal cycle evident at these two wavelengths which can be due to the low aerosol concentrations present in air masses from the Southern Ocean [31]. The 500 and 862 nm wavelengths were excluded due to missing data in the data set. The largest daily variability occurred during the austral summer which could be due to biomass burning in the surrounding areas [32].

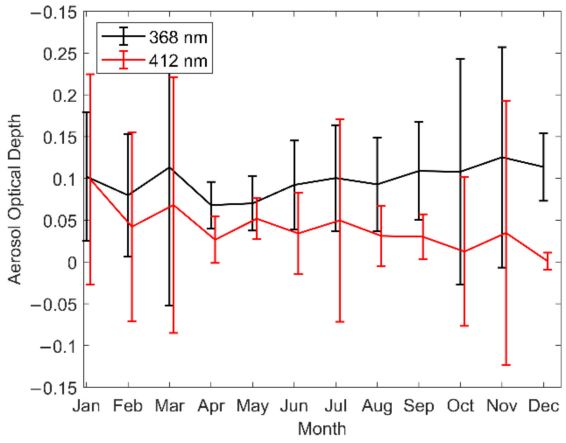

Figure 3. Monthly mean and ± 1 standard deviation (SD) error bars of aerosol optical depth (AOD) from precision filter radiometer (PFR) measurements for 368 and 412 nm at Cape Point.

The daily mean of PFR AOD at 368 and 412 nm (Figure 4) showed an increase in AOD between 9 June and 13 June 2011 as well as on 27 June 2011. These values were above their respective monthly mean.

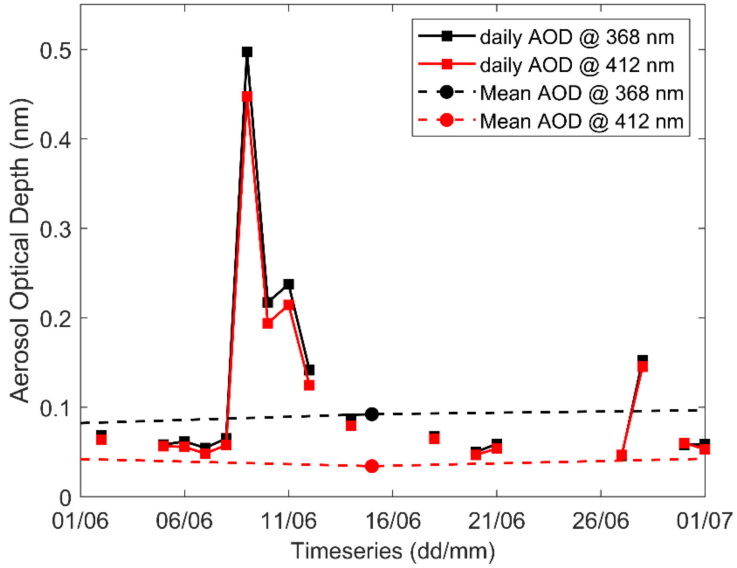

Figure 4. Daily mean and monthly mean of PFR measurements during May–July 2011 at 368 and 412 nm at Cape Point.

At the eruption site, the mean monthly and mean daily MERRA-2 SO_2 columns (Figure 5a) indicated a seasonal peak which occurred between February and April. During June and July 2011, the highest SO_2 level (3.7×10^{-5} kg·m^{-2}) was recorded on 5 June 2011 (Figure 5b), the day after the eruption started. The monthly mean for 2011 was above the climatological mean and there was increased variability during June and July 2011.

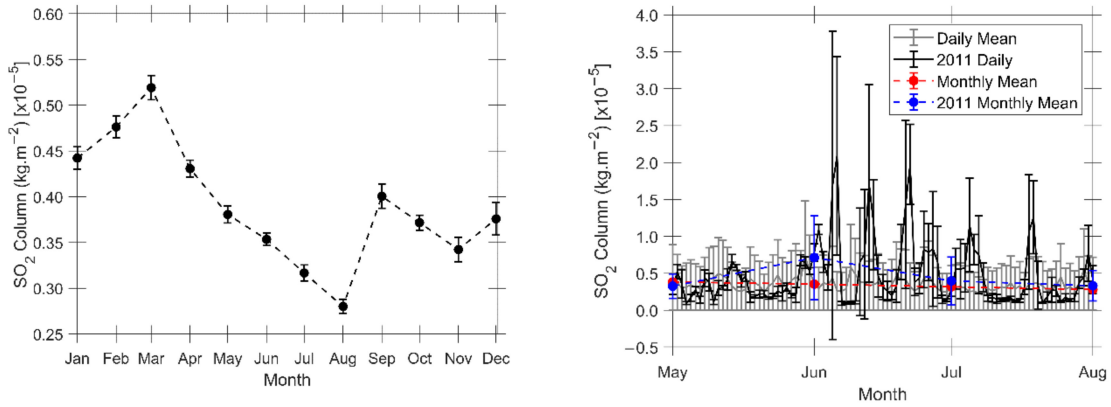

(a) (b)

Figure 5. Monthly mean and ± 1 SD for each month (2007–2016) (**a**) and daily mean and ± 1 SD error bars during May–July 2011 (**b**) for SO_2 column from Modern-Era Retrospective Analysis for Research and Applications version 2 (MERRA-2) at the Puyehue-Cordón Caulle volcanic complex (PCCVC).

At the secondary site, the SO_2 columns (Figure 6) were one order of magnitude smaller compared to the eruption site. The mean monthly and ± 1 SD error bars of SO_2 column (Figure 6a) showed a peak and increased variability during June to August. At Cape Point, SO_2 columns showed an increase from autumn months and reached a maximum during winter. The maximum was followed by a decrease during the spring months. In June and July 2011 (Figure 6b), the daily mean values were below the monthly mean values. However, between 10 and 20 June 2011 there was large variability in daily mean values. Between 12 June to 20 June 2011, the daily mean was above the climatological mean except for 15 June. During July 2011, there was a large increase in SO_2. The climatological seasonal variations of SO_2 were found to be as expected for a Southern Hemisphere site [33]. The increase during autumn, peaking in winter, and decreasing from spring into summer months may be due to the typical, prevailing synoptic circulation patterns [31].

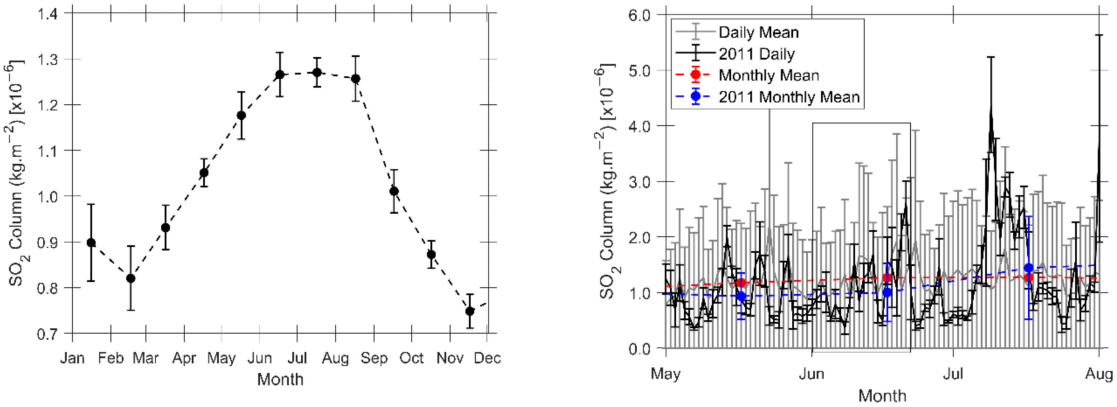

(a) (b)

Figure 6. Monthly mean and ± 1 SD for each month (2007–2016) (**a**) and daily mean and ± 1 SD error bars during May–July 2011, with 10–20 June 2011 indicated in the rectangle (**b**) for SO_2 column from MERRA-2 at Cape Point.

3.3. Infrared Atmospheric Sounding Interferometer (IASI) and Flexible Particle Model (FLEXPART)

The composite images of IASI SO_2 column (Figure 7), IASI ash (Figure 8) and FLEXPART SO_2 column (Figure 9) for 4–30 June 2011 shows the trajectory of the plume across the Southern Hemisphere.

The SO_2 column from IASI and FLEXPART indicated that the highest concentrations of SO_2 were found closest to the eruption site and decreased eastward. FLEXPART shows higher dispersion near the release point. The IASI ash observations showed a similar result compared to the SO_2 column observations but showed more longitudinal dispersion.

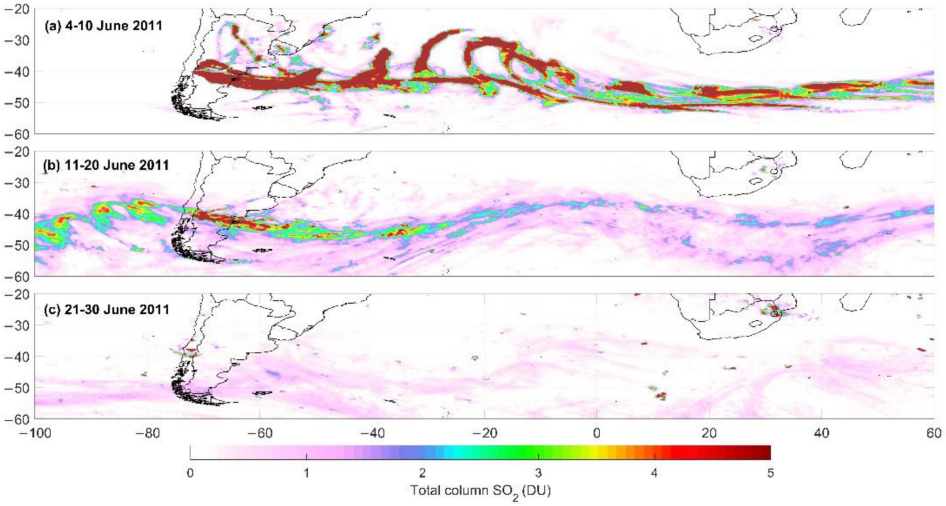

Figure 7. Composite image of Infrared Atmospheric Sounding Interferometer (IASI) SO_2 column for 4–10 June 2011 (**a**), 11–20 June 2011 (**b**) and 21-30 June 2011 (**c**).

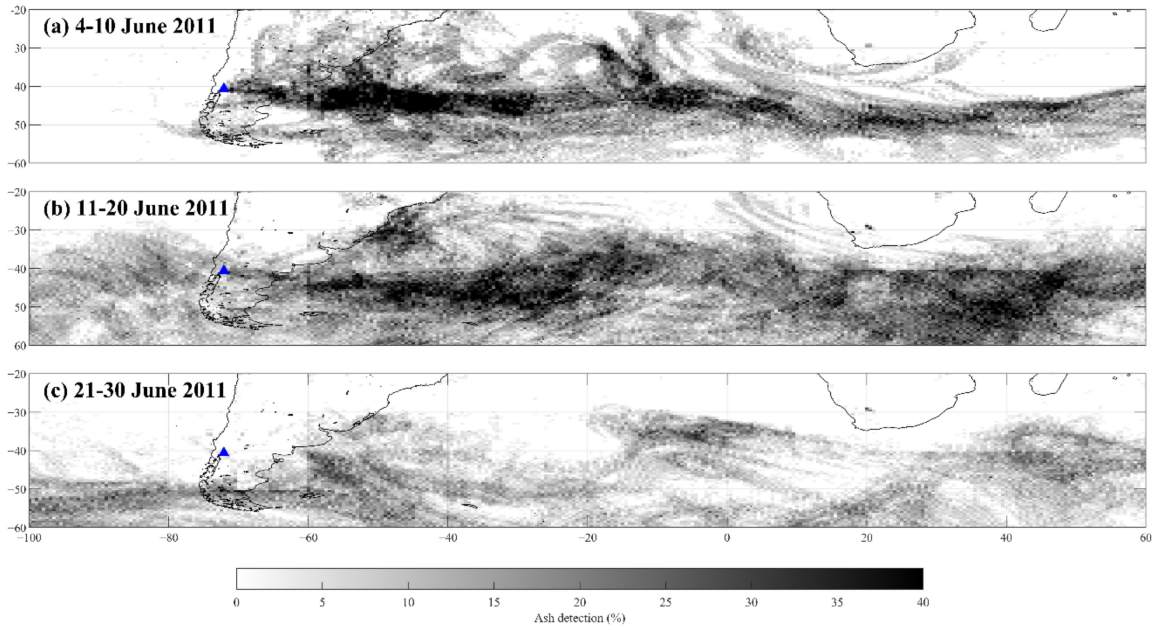

Figure 8. Composite image of IASI ash for 4–10 June 2011 (**a**), 11–20 June 2011 (**b**) and 21–30 June 2011 (**c**).

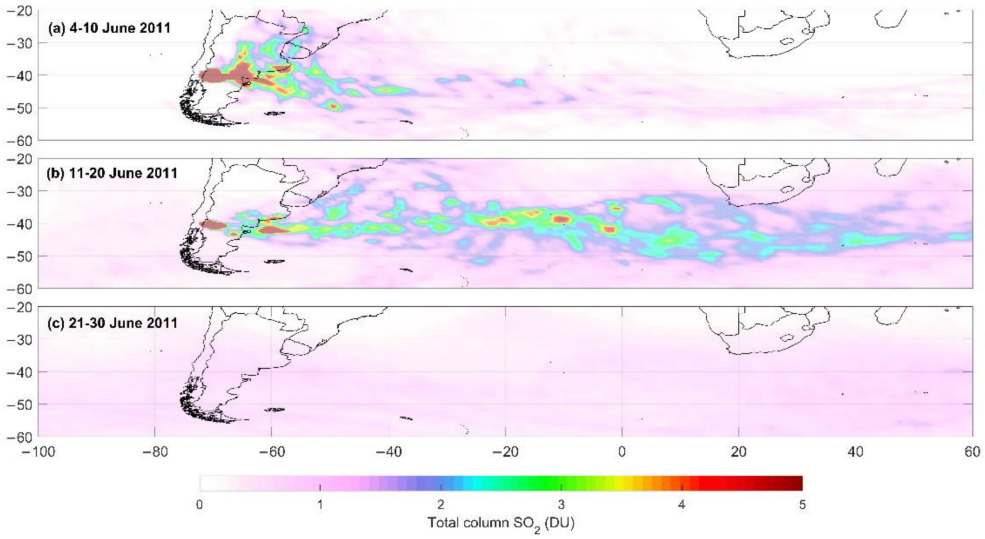

Figure 9. Composite image of flexible particle model (FLEXPART) SO_2 column for 4–10 June 2011 (**a**), 11–20 June 2011 (**b**) and 21–30 June 2011 (**c**).

The composite image of IASI SO_2 column (Figure 7a), IASI ash (Figure 8a) and FLEXPART SO_2 column (Figure 9a) for 4–10 June 2011 indicated that most of the plume was located between 20° S and 60° S. The SO_2 column from IASI and FLEXPART showed that the plume did not pass over Cape Point, but the IASI ash observations showed a low percentage ash near Cape Point. The composite image of the IASI SO_2 column (Figure 7b), IASI ash (Figure 8b) and FLEXPART SO_2 column (Figure 9b) for 11–20 June 2011 indicated that the plume had circumnavigated the Southern Hemisphere. During this period, the IASI and FLEXPART showed low levels of SO_2 and ash near Cape Point. This was more evident in the FLEXPART and IASI ash observations. The composite image of the IASI SO_2 column (Figure 7c), IASI ash (Figure 8c) and FLEXPART SO_2 column (Figure 9c) for 21–30 June 2011 each showed more dispersion and lower levels of SO_2 and ash compared to the period between 11–20 June 2011.

Comparing the plume from IASI observations and FLEXPART simulations showed similarities with this and other studies in the trajectory of the plume. A similar eastward transport was seen from the eruption site towards the Indian Ocean while most of the plume was distributed between 40°–60° S. From both IASI and FLEXPART a north-eastwards trajectory was seen on 4–10 June 2011 which resulted in the volcanic ash transport over Buenos Aires [9]. The dominant eastward trajectory and location of the plume south of Cape Point as indicated by the IASI and FLEXPART results agreed with results from other studies [23,26,27].

There were differences in dispersion results produced by IASI and FLEXPART, which were likely due to several factors. Lower volcanic emission after 10 June 2011 meant that IASI was not able to detect the eruption after this date [26]. In FLEXPART, the resolution of the meteorological data, number of particles released, mass, atmospheric lifetime of chemical species and changes in emissions would have had an impact on the FLEXPART simulation [4]. Furthermore, in high wind-shear environments ash and SO_2 follow different trajectories due to the deposition of ash [29].

The dispersion of the volcanic plume across the Southern Hemisphere did not have a large impact on surface UVR between 20° S and 60° S. This could be due to factors such as cloud cover and stratospheric ozone [34]. Furthermore, the eruption occurred during the austral winter when UVR are low. Although an increase in AOD was observed between 9–13 June 2011 at Cape Point. It is likely that the increase in AOD was due to the dispersion of volcanic ash (Figure 8) and not SO_2 as the dispersion of these particles vary depending on prevailing weather conditions. Furthermore, due to the danger that volcanic ash poses to aircraft, flights to and from Cape Town International Airport were affected between 9–19 June 2011 [35].

4. Conclusions

The dispersion of the volcanic plume from the PCCVC eruption on 4 June 2011 was investigated using satellite observations as well as a dispersion model. The observations and simulations were used to determine whether changes in surface solar UVR levels, AOD and SO_2 at the eruption site and a secondary, mid-latitude site could be attributed to the volcanic plume.

Over South America, the volcanic aerosols had an impact on surface solar UVR levels which was largely dependent on the wavelength. At the secondary site, Cape Point, increases in SO_2 column and AOD at 368 and 412 nm occurred between 10 June 2011 and 20 June 2011. The increase in AOD was likely due to the dispersion of volcanic ash. Satellite observations showed low levels of SO_2 near Cape Point, the secondary site. Future research should investigate the effect of volcanic aerosols using radiative transfer models.

Author Contributions: Conceptualization, D.J.D.P., H.B., N.B., R.F.H. and C.Y.W.; writing—original draft preparation, D.J.D.P., H.B., N.B., R.F.H. and C.Y.W.; UVI, PFR, MERRA-2 data analysis, D.J.D.P.; IASI data analysis, D.J.D.P., L.C.; FLEXPART modelling, D.J.D.P., N.B.; writing—review and editing, All authors. All authors have read and agreed to the published version of the manuscript.

Funding: D.J.D.P received a Doctoral scholarship from the University of Pretoria and a scholarship from the French Embassy in South Africa. C.W. receives research funding from the South African Medical Research Council, the National Research Foundation and the University of Pretoria. The APC was funded by LACy (Laboratoire de l'Atmosphère et des Cyclones).

Acknowledgments: The authors would like to acknowledge the initial work started by R.H and the Casper Labuschagne from the South African Weather Service for providing the PRF data from Cape Point. Authors acknowledge the French South-African PROTEA programme and the CNRS-NRF International Research Project ARSAIO (Atmospheric Research in Southern Africa and Indian Ocean), for supporting research activities.

Conflicts of Interest: The authors declare no conflict of interest.

References

1. Roberts, T.J.; Vignelles, D.; Liuzzo, M.; Giudice, G.; Aiuppa, A.; Coltelli, M.; Salerno, G.; Chartier, M.; Couté, B.; Berthet, G.; et al. The primary volcanic aerosol emission from Mt Etna: Size-resolved particles with SO2 and role in plume reactive halogen chemistry. *Geochim. Cosmochim. Acta* **2018**, *222*, 74–93. [CrossRef]
2. Daag, A.S.; Tubianosa, B.S.; Newhall, C.; Tungol, N.; Javier, D.; Dolan, M.; Delos Reyes, P.; Arboleda, R.; Martinez, M.; Regalado, T. Monitoring sulfur dioxide emission at Mount Pinatubo. In *Fire and Mud: Eruptions and lahars of Mount Pinatubo, Philippines*; University of Washington: Seattle, WA, USA, 1996; pp. 409–414.
3. Halmer, M.M.; Schmincke, H.U.; Graf, H.F. The annual volcanic gas input into the atmosphere, in particular into the stratosphere: A global data set for the past 100 years. *J. Volcanol. Geotherm. Res.* **2002**, *115*, 511–528. [CrossRef]
4. Klüser, L.; Erbertseder, T.; Meyer-Arnek, J. Observation of volcanic ash from Puyehue-Cordón Caulle with IASI. *Atmos. Meas. Tech.* **2013**, *6*, 35. [CrossRef]
5. Bignami, C.; Corradini, S.; Merucci, L.; de Michele, M.; Raucoules, D.; De Astis, G.; Stramondo, S.; Piedra, J. Multisensor Satellite Monitoring of the 2011 Puyehue-Cordon Caulle Eruption. *IEEE J. Sel. Topics Appl. Earth Observ. Remote Sens.* **2014**, *7*, 2786–2796. [CrossRef]
6. Robock, A. Volcanic eruptions and climate. *Rev. Geophys* **2000**, *38*, 191–219. [CrossRef]
7. Diaz, S.B.; Paladini, A.A.; Braile, H.G.; Dieguez, M.C.; Deferrari, G.A.; Vernet, M.; Vrsalovic, J. Global and direct UV irradiance variation in the Nahuel Huapi National Park (Patagonia, Argentina) after the eruption of Puyehue-Cordon Caulle (Chile). *J. Atmospheric Sol. Terr. Phys* **2014**, *112*, 47–56. [CrossRef]
8. Carn, S.A.; Krotkov, N.A. Chapter 12—Ultraviolet Satellite Measurements of Volcanic Ash. In *Volcanic Ash*; Mackie, S., Cashman, K., Ricketts, H., Rust, A., Watson, M., Eds.; Elsevier: Amsterdam, The Netherlands, 2016; pp. 217–231.
9. Raga, G.B.; Baumgardner, D.; Ulke, A.G.; Torres Brizuela, M.; Kucienska, B. The environmental impact of the Puyehue–Cordon Caulle 2011 volcanic eruption on Buenos Aires. *Nat. Hazards Earth Syst. Sci.* **2013**, *13*, 2319–2330. [CrossRef]

10. Bonadonna, C.; Pistolesi, M.; Cioni, R.; Degruyter, W.; Elissondo, M.; Baumann, V. Dynamics of wind-affected volcanic plumes: The example of the 2011 Cordón Caulle eruption, Chile. *J. Geophys. Res. Solid Earth* **2015**, *120*, 2242–2261. [CrossRef]
11. Silva Parejas, C.; Lara, L.; Bertin, D.; Amigo, A.; Orozco, G. The 2011-2012 eruption of Cordón Caulle volcano (Southern Andes): Evolution, crisis management and current hazards. Proceedings of EGU General Assembly Conference Abstracts, Vienna, Austria, 22–27 April 2012; p. 9382.
12. Brunke, E.-G.; Labuschagne, C.; Scheel, H.E. Trace gas variations at Cape Point, South Africa, during May 1997 following a regional biomass burning episode. *Atmos. Environ.* **2001**, *35*, 777–786. [CrossRef]
13. Hovila, J.; Arola, A.; Tamminen, J. *OMI/Aura Surface UVB Irradiance and Erythemal Dose Daily L3 Global Gridded 1.0 degree x 1.0 degree V3*; NASA Goddard Space Flight Center, Ed.; Goddard Earth Sciences Data and Information Services Center (GES DISC): Greenbelt, MD, USA, 2013. [CrossRef]
14. Brogniez, C.; Auriol, F.; Deroo, C.; Arola, A.; Kujanpää, J.; Sauvage, B.; Kalakoski, N.; Pitkänen, A.; Riku, M.; Catalfamo, M. Validation of satellite-based noontime UVI with NDACC ground-based instruments: Influence of topography, environment and satellite overpass time. *Atmos. Chem. Physics* **2016**, *16*. [CrossRef]
15. Fioletov, V.; Kerr, J.B.; Fergusson, A. The UV index: Definition, distribution and factors affecting it. *Can. J. Public Health* **2010**, *101*, I5–I9. [CrossRef] [PubMed]
16. Cadet, J.-M.; Bencherif, H.; Portafaix, T.; Lamy, K.; Ncongwane, K.; Coetzee, G.J.R.; Wright, C.Y. Comparison of Ground-Based and Satellite-Derived Solar UV Index Levels at Six South African Sites. *Int. J. Environ. Res. Public Health* **2017**, *14*, 1384. [CrossRef]
17. McArthur, L.J.B.; Halliwell, D.H.; Niebergall, O.J.; O'Neill, N.T.; Slusser, J.R.; Wehrli, C. Field comparison of network Sun photometers. *J. Geophys. Res. Atmos.* **2003**, *108*. [CrossRef]
18. Nyeki, S.; Halios, C.H.; Baum, W.; Eleftheriadis, K.; Flentje, H.; Gröbner, J.; Vuilleumier, L.; Wehrli, C. Ground-based aerosol optical depth trends at three high-altitude sites in Switzerland and southern Germany from 1995 to 2010. *J. Geophys. Res. Atmos.* **2012**, *117*, D18202. [CrossRef]
19. Smirnov, A.; Holben, B.; Eck, T.; Dubovik, O.; Slutsker, I. Cloud-screening and quality control algorithms for the AERONET database. *Remote Sens. Environ.* **2000**, *73*, 337–349. [CrossRef]
20. Greene, C.A.; Thirumalai, K.; Kearney, K.A.; Delgado, J.M.; Schwanghart, W.; Wolfenbarger, N.S.; Thyng, K.M.; Gwyther, D.E.; Gardner, A.S.; Blankenship, D.D. The climate data toolbox for MATLAB. *Geochem. Geophys. Geosystems* **2019**, *20*, 3774–3781. [CrossRef]
21. Global Modeling and Assimilation Office (GMAO). *MERRA-2 tavg1_2d_aer_Nx: 2d,1-Hourly, Time-averaged, Single-Level, Assimilation, Aerosol Diagnostics V5.12.4*; Goddard Earth Sciences Data and Information Services Center (GES DISC): Greenbelt, MD, USA, 2015. [CrossRef]
22. Ukhov, A.; Mostamandi, S.; Krotkov, N.; Flemming, J.; da Silva, A.; Li, C.; Fioletov, V.; McLinden, C.; Anisimov, A.; Alshehri, Y.M.; et al. Study of SO Pollution in the Middle East Using MERRA-2, CAMS Data Assimilation Products, and High-Resolution WRF-Chem Simulations. *J. Geophys. Res. Atmos.* **2020**, *125*, e2019JD031993. [CrossRef]
23. Clarisse, L.; Hurtmans, D.; Clerbaux, C.; Hadji-Lazaro, J.; Ngadi, Y.; Coheur, P.F. Retrieval of sulphur dioxide from the infrared atmospheric sounding interferometer (IASI). *Atmos. Meas. Tech.* **2012**, *5*, 581–594. [CrossRef]
24. Clarisse, L.; Prata, F. Infrared sounding of volcanic ash. In *Volcanic ash: Methods of observation and monitoring*; Mackie, S., Cashman, K., Ricketts, H., Rust, A., Watson, M., Eds.; Elsevier: Amsterdam, The Netherlands, 2015.
25. Moxnes, E.D.; Kristiansen, N.I.; Stohl, A.; Clarisse, L.; Durant, A.; Weber, K.; Vogel, A. Separation of ash and sulfur dioxide during the 2011 Grímsvötn eruption. *J. Geophys. Res. Atmos.* **2014**, *119*, 7477–7501. [CrossRef]
26. Theys, N.; Campion, R.; Clarisse, L.; Brenot, H.; van Gent, J.; Dils, B.; Corradini, S.; Merucci, L.; Coheur, P.F.; Van Roozendael, M.; et al. Volcanic SO_2 fluxes derived from satellite data: A survey using OMI, GOME-2, IASI and MODIS. *Atmos. Chem. Phys.* **2013**, *13*, 5945–5968. [CrossRef]
27. Carboni, E.; Grainger, R.G.; Mather, T.A.; Pyle, D.M.; Thomas, G.E.; Siddans, R.; Smith, A.J.A.; Dudhia, A.; Koukouli, M.E.; Balis, D. The vertical distribution of volcanic SO2 plumes measured by IASI. *Atmos. Chem. Phys.* **2016**, *16*, 4343–4367. [CrossRef]
28. Pisso, I.; Sollum, E.; Grythe, H.; Kristiansen, N.; Cassiani, M.; Eckhardt, S.; Arnold, D.; Morton, D.; Thompson, R.L.; Groot Zwaaftink, C.D.; et al. The Lagrangian particle dispersion model FLEXPART version 10.3. *Geosci. Model Dev.* **2019**, *2019*, 1–67. [CrossRef]

29. Walker, J.C.; Carboni, E.; Dudhia, A.; Grainger, R.G. Improved detection of sulphur dioxide in volcanic plumes using satellite-based hyperspectral infrared measurements: Application to the Eyjafjallajökull 2010 eruption. *J. Geophys. Res. Atmos.* **2012**, *117*. [CrossRef]
30. Eckhardt, S.; Prata, A.J.; Seibert, P.; Stebel, K.; Stohl, A. Estimation of the vertical profile of sulfur dioxide injection into the atmosphere by a volcanic eruption using satellite column measurements and inverse transport modeling. *Atmos. Chem. Phys.* **2008**, *8*, 3881–3897. [CrossRef]
31. Nyeki, S.; Wehrli, C.; Gröbner, J.; Kouremeti, N.; Wacker, S.; Labuschagne, C.; Mbatha, N.; Brunke, E.G. The GAW-PFR aerosol optical depth network: The 2008–2013 time series at Cape Point Station, South Africa. *J. Geophys. Res. Atmos.* **2015**, *120*, 5070–5084. [CrossRef]
32. Tesfaye, M.; Sivakumar, V.; Botai, J.; Mengistu Tsidu, G. Aerosol climatology over South Africa based on 10 years of Multiangle Imaging Spectroradiometer (MISR) data. *J. Geophys. Res. Atmos.* **2011**, *116*. [CrossRef]
33. Balashov, N.V.; Thompson, A.M.; Piketh, S.J.; Langerman, K.E. Surface ozone variability and trends over the South African Highveld from 1990 to 2007. *J. Geophys. Res. Atmos.* **2014**, *119*, 4323–4342. [CrossRef]
34. Kerr, J.B. Understanding the factors that affect surface ultraviolet radiation. *Optical Eng.* **2005**, *44*, 041002. [CrossRef]
35. Günther, T.; Schulze, M.; Friederici, A.; Theisel, H. Visualizing Volcanic Clouds in the Atmosphere and Their Impact on Air Traffic. *IEEE Comput. Graph. Appl.* **2016**, *36*, 36–47.